Chemical Science

Accepted Manuscript

This article can be cited before page numbers have been issued, to do this please use: K. Wang, V. Khare, A. A. Das, F. Razaviamri and B. P. Lee, *Chem. Sci.*, 2026, DOI: 10.1039/D5SC07881D.

ROYAL SOCIETY OF CHEMISTRY

rsc.li/chemical-science

View Article Online
DOI: 10.1039/D5SC07881D

Salicylhydroxamic acid as an electro-responsive and switchable adhesive molecule

*Kan Wang, Vedika Khare, Abhilash Arjan Das, Seyedehfatemeh Razaviamri, and Bruce P. Lee**

Biomedical Engineering Department, Michigan Technological University, 1400 Townsend Drive, Houghton, Michigan, 49931, United States

KEYWORDS: SHAM, electrochemistry, switchable adhesive, electro-responsive adhesion, wet adhesion, metal-ligand chelation

ABSTRACT: This study investigated salicylhydroxamic acid (SHAM) as a new electro-responsive, switchable adhesive molecule for wet adhesive contact. SHAM-containing polymer was synthesized and evaluated using a customized Johnson-Kendall-Roberts (JKR) contact mechanics setup, where a titanium (Ti) hemisphere simultaneously functioned as the contact substrate and cathodic electrode. Application of electrical potential (0.5–2V) for 30 s or less reduced the work of adhesion by 84%, while subsequent incubation in pH 5 buffer restored the original work of adhesion value. Unlike catechol-containing polymer, which underwent irreversible oxidation to quinone, SHAM demonstrated fully reversible switching without the need for a protective group. Cyclic voltammetry and electrochemical impedance spectroscopy

View Article Online
DOI: 10.1039/D5SC07881D

confirmed that both SHAM- and catechol-containing polymers exhibited comparable electrical conductivity, ensuring that the observed differences in adhesion behaviors stemmed from their intrinsic molecular properties. The combination of UV-vis, Fourier transform infrared, and X-ray photon spectroscopy experiments confirmed that the switching mechanism arose from protonation and deprotonation of SHAM, which regulated SHAM's ability to bond to the Ti surface. Conversely, catechol irreversibly oxidized to the poorly adhesive quinone form and failed to regain its initial adhesive property. SHAM exhibited electro-responsive interfacial bonding capability to a metallic surface under wet conditions and is potentially suitable for designing new switchable adhesives.

1. INTRODUCTION

Switchable adhesives with tunable, on-demand adhesion have attracted considerable interests for their potential to advancing research fields ranging from biomedical devices to robotic manipulation and wearable electronics[1-4]. By enabling reversible bonding and detachment under external stimuli (e.g., light, temperature, pH, and electric fields), these materials offer a sustainable strategy to reduce material waste, streamline assembly and disassembly, and minimize substrate damage during removal[5, 6]. However, many sources of external stimuli have limitations and are not practical. For example, light-responsive adhesives are limited to adhesive joints formed using transparent substrates[7] while thermo-responsive adhesives may require excessive heat leading to surface damage[8]. pH-triggered adhesion systems are inherently diffusion limited, with a slow switching rate between adhesive and non-adhesive states[9]. In contrast, electrical stimulation offers superior controllability, ease of operation, and seamless

View Article Online
DOI: 10.1039/D5SC07881D

integration with electronic devices[3, 10, 11]. Yet, most electro-responsive adhesives still require high voltage levels, making it challenging to balance strong adhesion with low-energy debonding[12]. This challenge highlights the critical need for electro-responsive adhesives that operate effectively at low voltages.

One general strategy in designing a switchable adhesive is the incorporation of a stimuli-responsive adhesive molecules into an adhesive polymer matrix[13]. A well-established example is the redox active catechol, which is one of the main adhesive molecules found in mussel foot proteins[14-16]. The adhesive property of catechol is highly dependent on its oxidation state where the reduced form of catechol demonstrates strong adhesion but is significantly weakened when oxidized into quinone[17]. Electrochemical oxidation of catechol can reduce its adhesion strength by up to 96%[18]. However, quinone is highly reactive and prone to irreversible crosslinking, which compromises reversibility[19]. To mitigate this limitation, we previously introduced boronic acid as a temporary protecting group to suppress irreversible catechol oxidation[20]. Catechol-boronic acid adhesives could be detached from metal substrates under applied electrical potential and partially regenerated through incubation in an acidic buffer[21]. However, it is difficult to completely dissociate the catechol-boronate complex to fully regain the initial adhesive property[9]. As such, there remains a pressing need for alternative adhesive molecules that combine strong and reversible adhesion that is responsive to applied electricity.

Salicylhydroxamic acid (SHAM) has recently emerged as a promising candidate as a switchable adhesive molecule and exhibits pH-responsive adhesion to wet surfaces (**Figure 1**)[22].

View Article Online
DOI: 10.1039/D5SC07881D

When incorporated into structural adhesives, SHAM achieved lap shear strengths that were significantly higher than catechol-based adhesives and a commercial epoxy glue[23]. Unlike catechol, SHAM features both a hydroxamic acid group and a phenolic hydroxyl group. Hydroxamic, bearing bidentate (O,O) donor sets, are well-known for strong metal chelation[24, 25]. For example, SHAM adhesion to titanium depends on its protonation state and can be reversibly modulated by pH[22]. Under basic conditions, deprotonated SHAM exhibits reduced adhesion, whereas protonation under acidic conditions restores full adhesion. In a typical electrochemical reaction, local accumulation of hydroxide (OH^-) and protons (H^+) near the cathode and anode, respectively, creates a pH gradient[26, 27], which could potentially be utilized to tune the adhesive property of SHAM.

In this study, we investigated the feasibility for SHAM to function as an electro-responsive, switchable adhesive molecule without the use of a protecting group. We synthesized SHAM-based adhesive consisting of a methoxyethyl methacrylate (MEA) backbone and a conductive pyrene moiety (**Figure 1c**). The adhesive was coated onto aluminum (Al) discs (serving as the anode), and the adhesive property of SHAM-containing polymer was characterized using Johnson-Kendall-Roberts (JKR) contact mechanics testing using a titanium (Ti) hemisphere (cathode) as the test substrate. The effect of applied electrical potential and exposure time on the adhesive property of SHAM-based adhesive (SHA) was determined and benchmarked against catechol-based polymer (CAT). In addition, UV-vis spectroscopy, Fourier transform infrared (FTIR) spectroscopy, and X-ray photon spectroscopy (XPS) were employed to characterize the redox state of adhesive moieties following electrical treatment, while cyclic voltammetry (CV)

View Article Online
DOI: 10.1039/D5SC07881D

and electrochemical impedance spectroscopy (EIS) were used to assess the conductivity of the adhesive coatings.

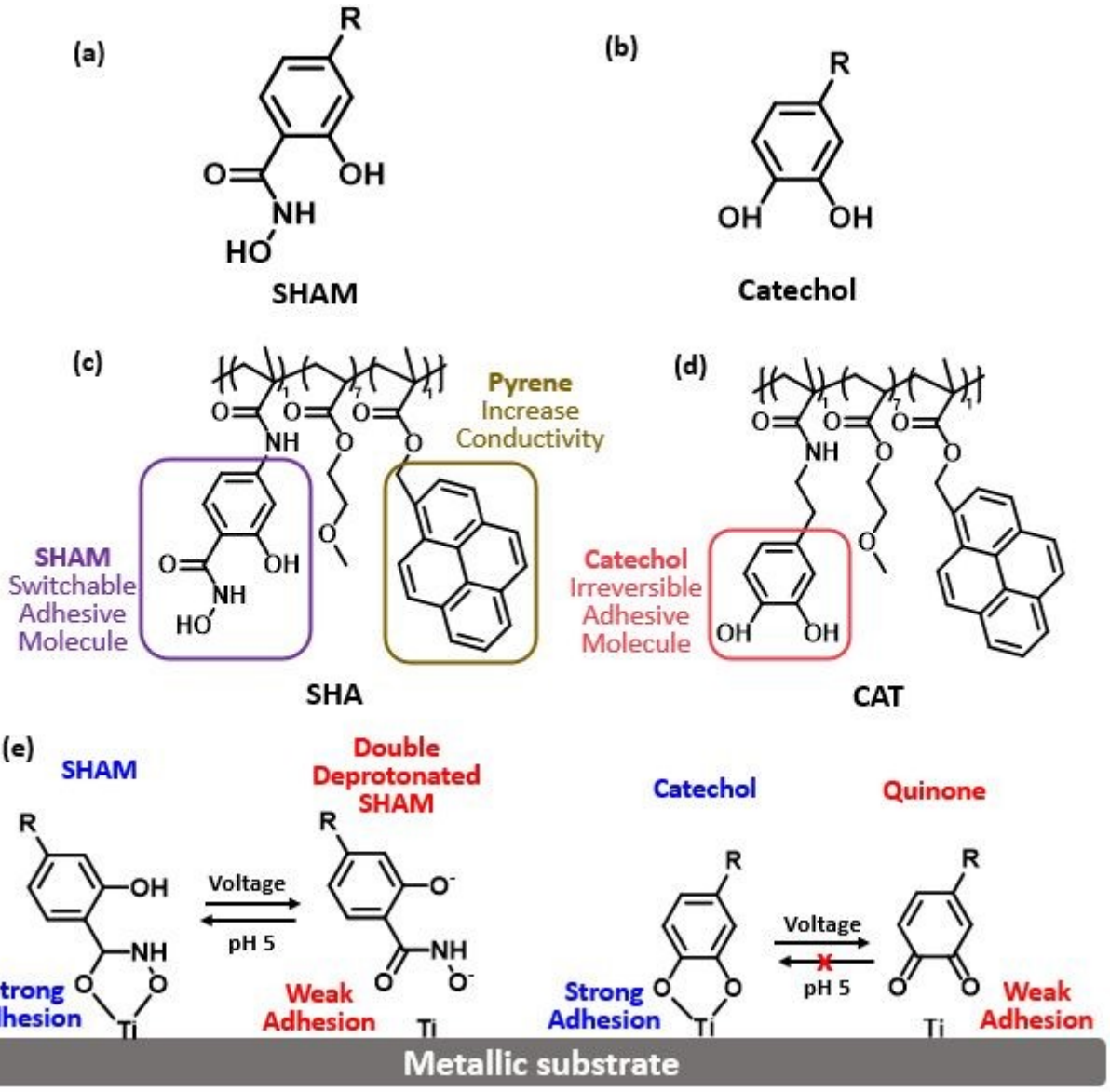

Figure 1. Chemical structures of (a) SHAM, (b) catechol, (c) SHAM-based polymer (SHA) and (d) catechol-based polymer (CAT). (e) Electrochemical deactivation of SHAM and catechol. SHAM could be reactivated with a mildly acidic solution while catechol becomes irreversibly oxidized without a protecting group.

View Article Online
DOI: 10.1039/D5SC07881D

2. MATERIALS AND METHODS

2.1. Materials.

MEA, 1-pyrenylmethyl methacrylate (PyMA), 1-methyl-2-pyrrolidinone (NMP), polyvinylidene fluoride (PVDF), silicon oil, dimethyl sulfoxide-d_6 (DMSO-d_6), hydrochloric acid (HCl), sodium hydroxide (NaOH), and sodium chloride (NaCl) were purchased from Sigma-Aldrich (St. Louis, MO). Dimethylformamide (DMF) and diethyl ether were purchased from Fisher Scientific (Fair Lawn, NJ). 2,2′-Azobis(isobutyronitrile) (AIBN) was purchased from Wako Pure Chemical Industries, Ltd. (Osaka, Japan). Ti ball (1/4" diameter), 303 stainless steel (SS) rod (1/2″ diameter), Al rods (1/2” and 3/8" diameters), copper wire, and polytetrafluoroethylene (PTFE) (3/8" diameter) were purchased from McMaster-Carr (Elmhurst, IL). SS and Al rods with a diameter of 1/2” were machined into hemispheres with a diameter of 5.9 mm. Al rod with a diameter of 3/8" was trimmed into Al plates using an 8026J Clausing/Colchester Manual Engine Lathe (Clausing Industrial; Kalamazoo, MI). The electrolyte was prepared using deionized (DI) water and 0.1 M NaCl, pH was adjusted to 7.4. Two adhesive monomers, *N*,2-dihydroxy-4-methacrylamidobenzamide (DHMAAB) and dopamine methacrylamide (DMA) were synthesized according to previously published protocols[18, 22].

2.2. Adhesive polymers preparation and characterization.

The adhesive polymers were prepared by thermo-initiated polymerization using AIBN as the initiator (**Figure S1**). To prepare the SHAM-based polymer (SHA), 10 mmol MEA (1.29 mL), 1 mmol DHMAAB (236 mg), 1 mmol PyMA (300 mg), and 0.3 mmol AIBN (49 mg) were dissolved in 10 mL DMF. The solution was stirred at 500 rpm and heated at 70%˚C in a silicon

View Article Online
DOI: 10.1039/D5SC07881D

oil bath under a nitrogen atmosphere overnight. The resulting polymer was precipitated in diethyl ether, filtered, and vacuum-dried for 24 hours. For comparison, a catechol-based copolymer (CAT) was synthesized using DMA instead of DHMAAB using a monomer ratio of 7:1:1:0.3. The chemical compositions of two adhesive polymers were investigated by proton nuclear magnetic resonance (^{1}H NMR) spectroscopy using an Ascend 500 MHz spectrometer (Bruker corporation; Billerica, MA). The weight-average molecular weight ($\overline{M}_w$), number-average molecular weight ($\overline{M}_n$), and polydispersity index (PDI) of the adhesive polymers were determined by gel permeation chromatography (GPC) using a Shimadzu Nexera HPLC system (Kyoto, Japan) equipped with a Shodex OHpak LB-803 column, a UV detector (SPD-40, Shimadzu), a refractive index detector (RID-20A, Shimadzu), and a multi-angle light scattering detector (miniDAWN, Wyatt). Polymer samples were dissolved in HPLC-grade DMSO at a concentration of 5%mg/mL and eluted at 0.5%mL/min using HPLC-grade DMF as the mobile phase at 40%˚C.

The absorption spectra of 0.2 mmol/L DHMAAB and DMA aqueous solutions at different pH levels were examined using UV-vis spectroscopy (LAMBDA35, PerkinElmer, MA). Spectra were first recorded after dissolving the monomers in 0.1 M NaCl solution (electrolyte) containing 0.2 mM of the adhesive monomer. To mimic the alkaline environment detected by pH strip during electrochemical deactivation, a small aliquot of 1 M NaOH solution (pH 14) was added to the cuvette to increase the solution pH to ~9. Subsequently, a small aliquot of 1 M HCl solution (pH 0) was introduced to reduce the solution pH to ~5, reproducing the recovery conditions and enabling evaluation of the reversibility of the adhesive molecules.

View Article Online
DOI: 10.1039/D5SC07881D

2.3. Adhesive-coating preparation and characterization.

The adhesive precursor solution was prepared by dissolving the adhesive polymer and PVDF in NMP at a weight ratio of 9:1 at final polymer concentrations of 100 and 11 mg/mL, respectively. 15%µL of precursor solution was pipetted onto an Al disc (3/8" diameter) and left in a fume hood overnight to allow complete evaporation of the NMP (**Figure S2**). The coated samples were vacuum dried and analyzed using FTIR spectroscopy (IRTracer-100, Shimadzu Corporation; Kyoto, Japan). The morphology of the coating was visualized using a Hitachi S-4700 field emission scanning electron microscope (FE-SEM, Tokyo, Japan).

To evaluate the electrochemical properties of the adhesive, 2 µL of precursor solution was deposited onto the working electrode (WE) of a commercial gold-coated interdigitated electrode (IDE, Medetronix Labs Pvt Ltd, Uttar Pradesh, India) while leaving the counter electrode (CE) and reference electrode (RE) uncoated (**Figure S3**). The coating was left to dry in a fume hood overnight. This process yielded a thin adhesive film with an area of approximately 7%mm^2 on the detection zone. Electrochemical measurements were performed in 10 mL of 0.1 M NaCl solution (pH 7.4), sufficient to submerge all electrodes. CV was carried out by sweeping the potential between -2%V and +2%V at a scan rate of 0.1%V/s. EIS was conducted using the same adhesive-coated IDE and electrolyte, with a perturbation amplitude of 5 mV/s over a frequency range of 0.1–10^6 Hz. The charge transfer resistance (R_c) of the adhesive coating was extracted from EIS spectrum. In Nyquist plots, the high-frequency intercept on the X axis corresponds to the solution resistance, while the second X-intercept, obtained by extending the semicircle at lower frequencies, reflects the combined resistance of ion and charge transfer. R_c was

View Article Online
DOI: 10.1039/D5SC07881D

determined as the difference between these two X-intercepts[21]. Both CV and EIS were performed using a VersaSTAT 3 Potentiostat Galvanostat (10−240 Vac; 50/60 Hz; 250 VA Max) from AMETEK Scientific Instruments (Berwyn, PA).

2.4. JKR contact mechanics tests.

The JKR testing device consisted of a custom-built PTFE indenter, a 10-g load cell (ALS-06, Transducer Techniques), and a high-resolution miniature linear stage stepper motor (MFA-PPD, Newport) (**Figure 2**). A Ti hemisphere was attached to the indenter with a copper wire embedded at the interface (**Figure 2d**). The adhesive surface was wetted with 15%μL of 0.1%M NaCl solution at pH 5 (**Figure 2e**). During contact testing, the Ti hemisphere was brought into contact with the adhesive-coated surface at a speed of 1%μm/s until a maximum preload of 10%mN. Then, the Ti hemisphere was retracted at the same speed. Based on a JKR model that illustrates a rigid spherical surface onto a thin coating on a rigid substrate, the work of adhesion (W_{adh}) equals to the critical energy release rate (G_c), the maximum adhesion force (F_{max}) and the radius (R) of the Ti tip were used to calculate the W_{adh}[28-30]:

$$W_{adh} = G_c = \frac{2}{3\pi R} F_{max} \text{(Equation 1)}$$

The initial adhesion, measured without any applied voltage, was recorded as the virgin adhesive property. To examine the effect of electrical potential, the pH 5 NaCl solution was replaced with a pH 7.4 NaCl solution. The Ti hemisphere was immersed in the solution and brought close to the adhesive without contacting the adhesive. The Ti hemisphere, electrolyte, adhesive-coated Al disc, and a Keithley 2460 Source Meter formed a complete electrical circuit.

View Article Online
DOI: 10.1039/D5SC07881D

Voltages between 0.1-2%V were applied for 15-45 seconds to deactivate the adhesive. After voltage application, the Ti hemisphere was brought into contact with the surface to determine F_{max} as described above. To recover the adhesive property of SHA, deactivated samples were incubated in 0.1%M NaCl solution at pH 5 for 30 minutes before performing another adhesive contact. Adhesive reversibility was assessed over five cycles of deactivation (1%V for 30%s) and recovery (30%mins). JKR experiments were also performed using SS and Al hemispheres to determine the interfacial bonding behavior of SHA to these metals and the ability for these metals to function as an electrode to deactivate the adhesive property of SHA.

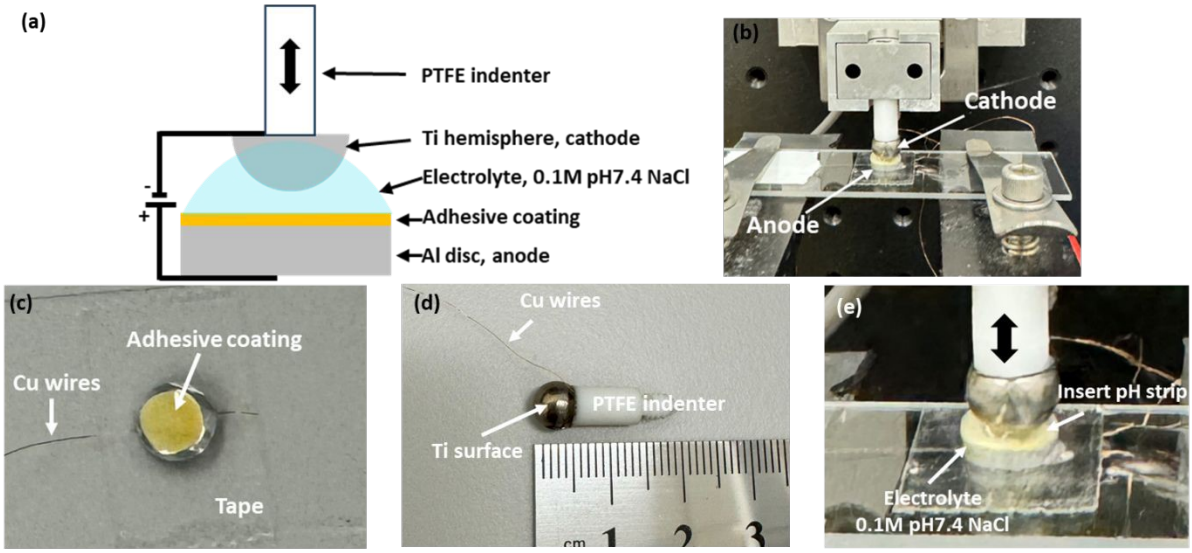

Figure 2. (a) Schematic representation and (b) photograph of the custom-built JKR setup used for adhesion testing with the application of electricity. Close views of the (c) anode, (d) cathode, and (e) interface of the adhesion testing.

2.5. XPS

15 µL of 100 mg/mL of adhesive polymer in NMP was applied onto Al discs (diameter 6.33 mm) and dried in a fume hood for 24 hours. To deactivate the adhesive, 15 µL of 0.1 M NaCl

View Article Online
DOI: 10.1039/D5SC07881D

(pH 7.5) was added to on the adhesive surface, a Ti disc (diameter 6.33 mm, cathode) was placed near the adhesive coating without making contact, and a voltage of 1 V was applied for a duration of 30 seconds using the Al disc as the anode. Reactivation was performed by incubating the coated discs in a pH 5 0.1 M NaCl solution for 30 minutes. The samples were vacuum dried before XPS measurements were conducted.

XPS spectra were obtained utilizing a PHI 5800 XPS system (Physical Electronics, Chanhassen, MN, USA) that features a dual Mg/Al X-ray source. Measurements were conducted utilizing Mg Kα radiation, with a photon energy of 1253.6 eV. Survey spectra were obtained using a pass energy of 187.85 eV, a step size of 0.8 eV, and a dwell time of 20 ms per step across a binding energy range of 0–1175 eV. High-resolution spectra of the C 1s and O 1s regions were acquired with a pass energy of 23.50 eV, a step size of 0.1 eV, and a dwell time of 100 ms for each step. Charge neutralization was implemented during the spectral acquisition process. All spectra were processed with CasaXPS software (Casa Software Ltd., Teignmouth, UK). Calibration of binding energy was conducted using the adventitious C–C/C=C peak at 284.8 eV as a reference. Peak fitting utilized Shirley background subtraction and a combination of Gaussian and Lorentzian peak shapes. The peak areas were normalized to the total envelope area, and the component fractions are reported as relative area percentages.

2.6. Statistical analysis.

One-way analysis of variance (one-way ANOVA) with Tukey method was used for comparing multiple groups, using a p-value of 0.05.

View Article Online
DOI: 10.1039/D5SC07881D

3. RESULTS AND DISCUSSION

3.1 Adhesive polymers and adhesive-coated Al discs preparation

Adhesive polymers were synthesized using a MEA backbone, adhesive monomers (DHMAAB for SHA and DMA for CAT), and the conductive monomer PyMA via thermally initiated free radical polymerization (**Figure S1**). The resulting polymers contained SHAM or catechol side chains, enabling switchable adhesion to metal surfaces. PyMA was incorporated to enhance conductivity through π-π stacking interactions from pyrene groups, thereby enhancing electron mobility and overall conductivity[21]. The chemical compositions of the copolymers were determined by ^{1}H NMR spectroscopy (**Figures S4** and **S5**). Characteristic peaks were observed for MEA (3.2-4.1 pm), the aromatic ring of catechol (6.4-6.7 ppm), the aromatic ring of SHAM (7.1-7.7 ppm), and pyrene (7.5-8.5 ppm). Integration of these peaks indicated that the molar ratios of MEA:adhesive monomer (DHMAAB or DMA): PyMA to be 7:1:1. The polymers were designated as SHA and CAT for SHAM- and catechol-containing copolymers, respectively. Based on GPC, SHA exhibited a significantly higher $\overline{M}_n$ (217 kDa) when compared to that of CAT (16.3 kDa) (**Tables S1**). The lower molecular weight of CAT may be due to the partial inhibition of the free-radical polymerization by the unprotected catechol[31]. Nevertheless, the SHAM and catechol contents in the two copolymers were both found to be ~11 mol% based on ^{1}H NMR spectra, and the difference in the MW will not affect the adhesion values measured based on JKR contact mechanics testing[32].

3.2 CV and EIS analysis

View Article Online
DOI: 10.1039/D5SC07881D

CV was performed over a potential range of ±2%V to investigate the redox behavior of the copolymers. SHA exhibited an anodic peak at +0.54%V, while CAT displayed a peak at +0.95%V, both corresponding to oxidation of their respective functional groups (**Figure 3** and **Table S2**). The lower anodic peak potential for SHAM indicated that it is easier to oxidize than catechol[33]. In contrast, SHA exhibited two cathodic peaks at -0.31%V and -0.98%V, while CAT showed peaks at -0.22%V and -0.85%V, suggesting that catechol undergoes reduction more readily than SHAM[33]. The peak current intensities of SHA and CAT were comparable, reflecting similar charge-transfer capacity. This is potentially due to similar PyMA content (~11 mol% based on ^{1}H NMR spectra) in both copolymers, which contributed to electron conductivity[21].

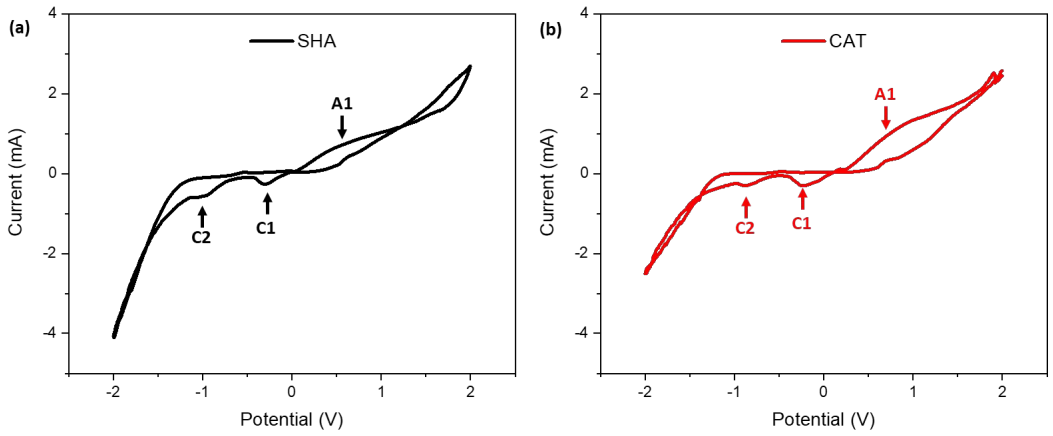

Figure 3. Cyclic voltammogram of (a) SHA and (b) CAT coated IDEs in 0.1M NaCl solution (pH 7.4) using a scan rate of 100 mV/s.

To further investigate the electronic properties of the copolymers, EIS was conducted on adhesive-coated IDEs (**Figure S6**). The Nyquist plots displayed a partial semicircle at the high-frequency region followed by a Warburg diffusion-related linear curve at lower frequencies[34, 35].

View Article Online
DOI: 10.1039/D5SC07881D

Although our recorded spectra did not display a complete semicircle due to our instrumental limitations, reliable R_c values were obtained through equivalent circuit fitting using the ZView software. R_c, which represents the electron transport across the electrode-electrolyte interface[34], was determined to be 34.5±4.5 Ω/mm² and 31.8±1.8 Ω/mm² for SHA and CAT, respectively. These values indicate that both copolymers exhibit comparable electrical conductivity, which minimizes the influence of polymer resistance to electrical stimulation. Thus, subsequent adhesion experiments primarily reflect the intrinsic adhesive performance of SHAM versus catechol, rather than confounding differences in electronic properties.

3.3 Effect of exposure time to electricity

The adhesive precursor solution was coated directly onto Al discs using PVDF as a binder to form a cohesive film on the Al surface. This procedure is consistent with methods used in battery electrodes, wearable electronics, and advanced coatings[36]. The coating thickness was measured by FE-SEM to be approximately 60 μm for both copolymers (**Figure S7**). The coating thickness was deliberately minimized to reduce electrical resistance, consistent with the reported inverse relationship between membrane resistance and thickness[37]. The interfacial bonding behavior and electro-responsiveness of the coatings were evaluated using JKR contact mechanics tests (**Figure 2**). A Ti hemisphere was employed both as the conductive electrode and the contact substrate. Ti serves as a representative model surface as both SHAM and catechol have previously been demonstrated to strong interfacial bonding to Ti[23]. The Al disc serves as the counter electrode due to its high conductivity and inherent corrosion resistance[38, 39]. 0.1%M NaCl was used as the

View Article Online
DOI: 10.1039/D5SC07881D

interfacial electrolyte to complete the circuit between electrodes, power supply, and conductive coating, while simultaneously serving as the aqueous medium for wet adhesion contact.

Prior to electrical stimulation, the virgin W_{adh} values for SHA and CAT coatings were determined to be 1.59±0.17 and 0.62±0.12 J/m^2, respectively (**Figures 4** and **S8**). The higher W_{adh} value of SHA indicates superior adhesion relative to CAT. Application of 0.1 V for up to 45 s did not significantly alter the calculated W_{adh} values, indicating that such a low potential was insufficient to deactivate adhesion in either polymer. At higher voltage levels, W_{adh} decreased progressively with increasing applied potential. For example, applying an electrical potential of 0.5, 1, and 2%V for 15 s reduced the W_{adh} values of SHA by approximately 37%, 76% and 77%, respectively, relative to the virgin state. Similarly, W_{adh} values also decreased proportionally with increasing exposure time for both adhesives. These results indicated that higher applied voltage and longer exposure time to applied electricity accelerated adhesion deactivation.

View Article Online
DOI: 10.1039/D5SC07881D

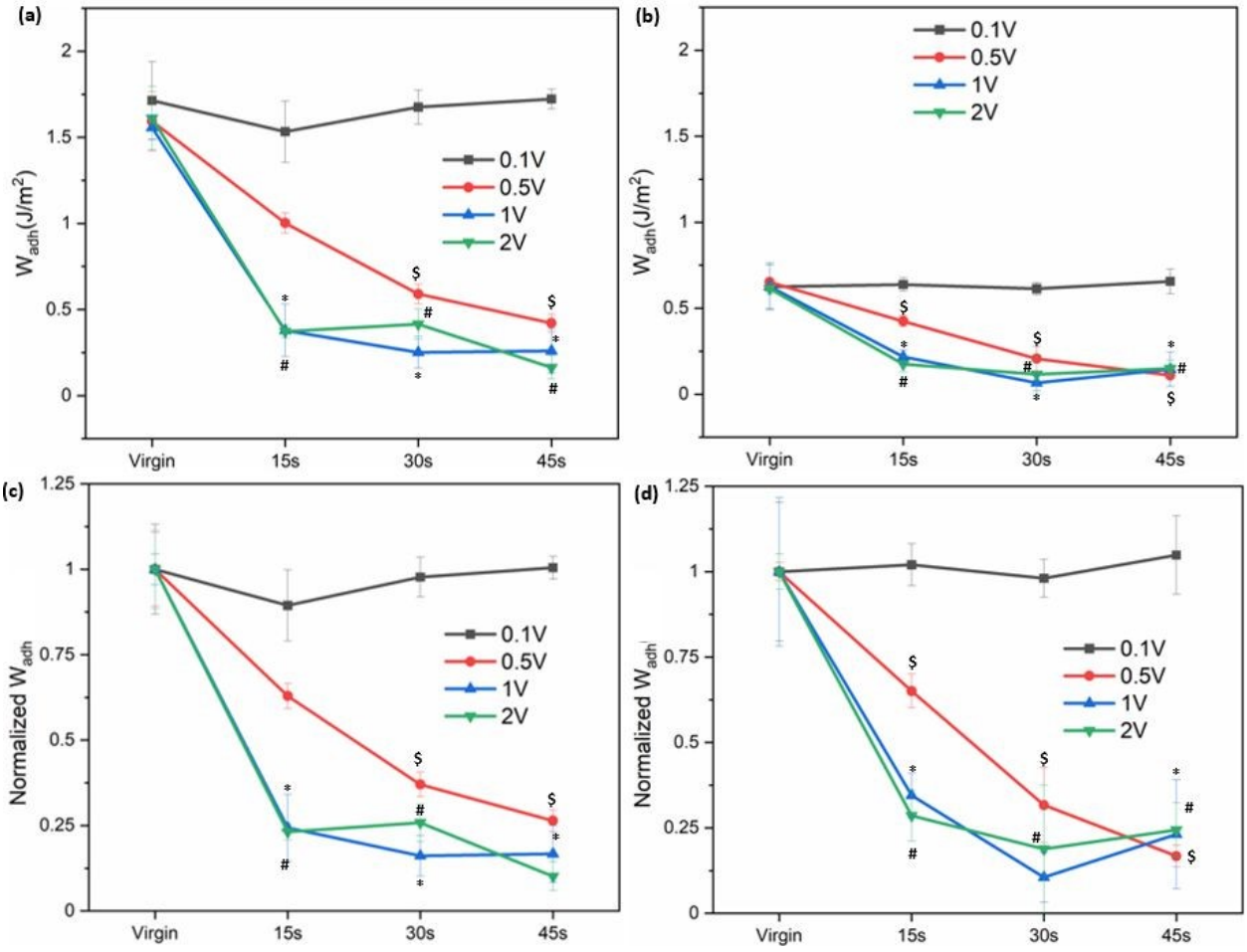

Figure 4. W_{adh} of (a) SHA and (b) CAT coating exposed to 0.1 V-2 V for different amounts of time in the presence of an electrolyte of pH 7.4. (c and d) W_{adh} values normalized to their average virgin adhesion values for SHA and CAT, respectively. $^{\%, \$, *, \#}p<0.05$ when compared to the virgin adhesive properties for 0.1, 0.5, 1, and 2V, respectively.

JKR experiments were also performed using SS and Al hemispheres to determine the interfacial bonding behavior of SHA coating to these metals and the ability for these metals to function as an electrode to deactivate SHA (**Figure S9**). Among the tested metals, SHA exhibited the highest virgin W_{adh} value when contacting Ti and the lowest value when contacting Al. This result corroborated well with previously reported density functional theory (DFT) calculations

View Article Online
DOI: 10.1039/D5SC07881D

where SHAM's binding energy with Ti (-200 kJ/mol) was much higher when compared to that with Al (-2 kJ/mol)[40, 41]. The strong adhesion between SHAM and Ti likely arises from the robust bidentate adsorption to the surface oxide[42], whereas the heterogeneous oxide layer on stainless steel may reduce the uniformity and strength of SHAM coordination[43]. After applying 1V for 30 seconds, the determined W_{adh} values of SHA decreased to around 0.3-0.4 J/m^2, a reduction of 81%, 72%, and 39% for Ti, SS, and Al, respectively. The different metals used here are highly electrically conductive for serving as an electrode (2.52, 1.36, and 37.7 MS/m for Ti, SS, and Al, respectively)[44], making bulk conductivity unlikely to govern their electrochemical response. The measured W_{adh} values after exposure to applied electricity maybe due to nonspecific interactions such as van der Waals forces, interfacial hydration, and contribution from incomplete removal of interfacial bonding[45], which may be the reason for similar W_{adh} values after electrical stimulation.

To evaluate whether electrochemically deactivated adhesives could recover their original adhesive property, samples were incubated in pH 5 buffer for 30 minutes following deactivation (**Figures 5** and **S10**). Since 0.1 V did not induce measurable deactivation, recovery experiments focused on samples that were exposed to 0.5–2%V. After 30 seconds of exposure to applied electricity, W_{adh} values for SHA decreased by 71–84% and fully recovered its initial adhesive property after incubation at pH 5. By contrast, CAT displayed a decrease in the W_{adh} value after exposure to applied voltage but did not recover. Instead, W_{adh} values further declined in the third contact cycle (84–97% decrease from the virgin adhesive). This indicated that catechol irreversibly oxidized.

View Article Online
DOI: 10.1039/D5SC07881D

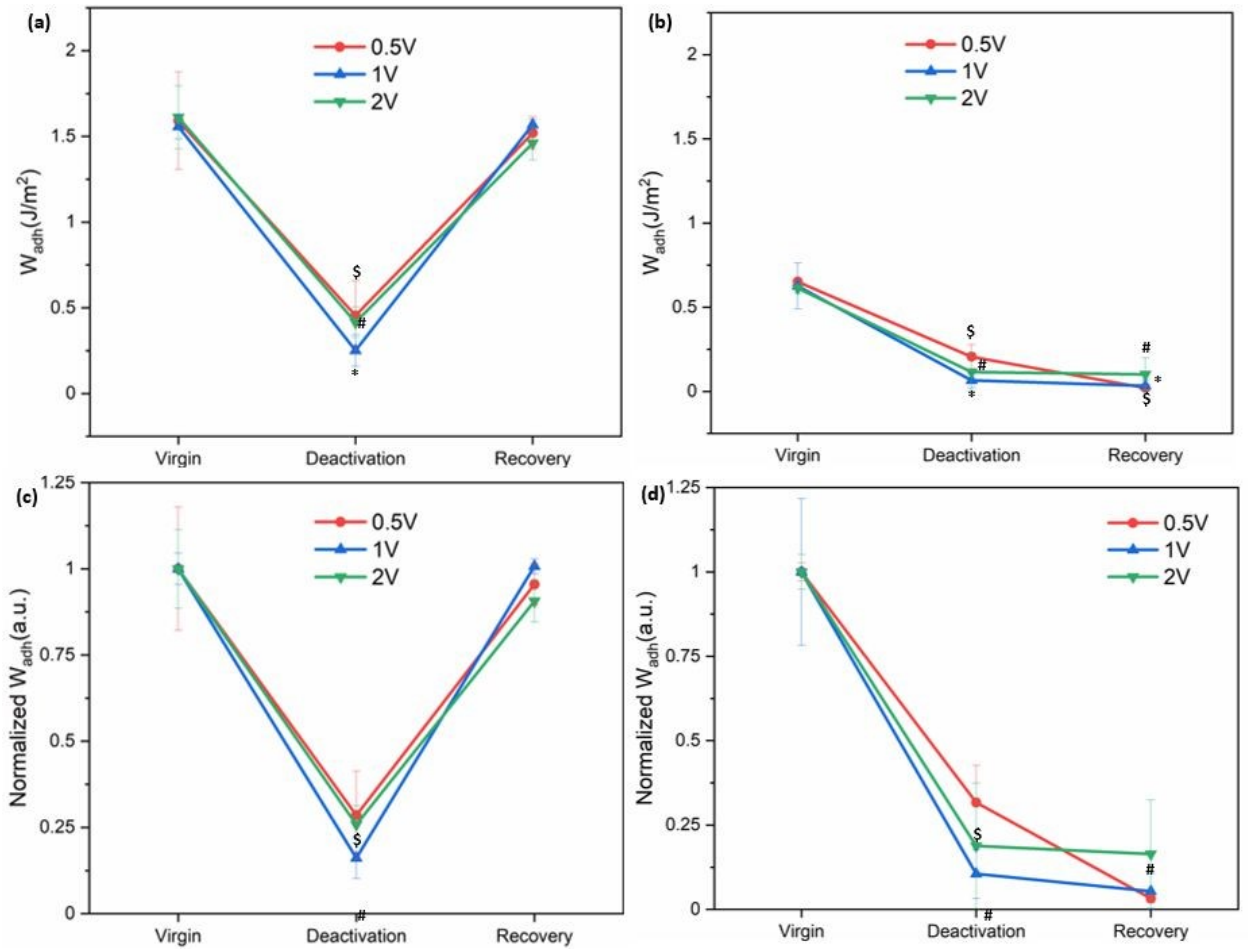

Figure 5. W_{adh} of (a) SHA and (b) CAT coating after deactivation with 0.5-2V for 30s and recovery through incubation in pH 5 buffer for 30 mins. (c and d) W_{adh} values normalized to their average virgin adhesion values for SHA and CAT, respectively. $^{\$, *, \#}p<0.05$ when compared to the virgin adhesive properties for 0.5, 1, and 2V, respectively.

In addition to recovery by incubation at pH 5, we attempted a more convenient method by reversing the polarity of the applied potential[20, 46]. As shown in **Figure S11**, the initial W_{adh} value was 1.66±0.24 J/m^2. After deactivation by applying 2 V for 30 s, adhesion decreased by 68%. Reversing the polarity by using Ti as the anode and Al as the cathode and applying 2 V for an

View Article Online
DOI: 10.1039/D5SC07881D

additional 30 s did not restore the original W_{adh} value. The failure to recover adhesion may be attributed to continued electron transfer under prolonged charging, which could induce isomerization of the SHAM chelate ligand and disrupt coordination with Ti, thereby preventing adhesion recovery[47, 48].

Video S1 demonstrates the deactivation and recovery of SHA. Initially, the SHA-coated Al disc adhered to the Ti hemisphere in the presence of electrolyte, confirming adhesive properties in a wetted condition. When the power supply was activated and the Ti electrode was connected as the cathode, application of 2 V caused the Al disc to detach within 2 seconds due to the loss of adhesion. The adhesive remained deactivated despite multiple contacts with the Ti hemisphere. After incubating in pH 5 buffer for 30 minutes, the Ti hemisphere was once again able to lift the Al disc, confirming full recovery of adhesion.

Litmus papers were used to track the changes in pH of the interfacial solution as a result of electrical stimulation (**Figure S12**). Application of 1 V for 30 s increased the pH at the interface from 7.4 to 9-10. The applied voltage generated a locally basic environment through water electrolysis[49]. This result indicated that the changes in pH contributed to adhesive deactivation. UV-vis spectroscopy was utilized to further investigate the effect of pH change on the adhesive molecules. The copolymers contain hydrophobic side chains (e.g., PyMA) and are poorly water soluble. As such, UV-vis spectra of DHMAAB and DMA were measured with sequentially changing the pH of the solution.

View Article Online
DOI: 10.1039/D5SC07881D

As shown in **Figure S13a**, DHMAAB displayed absorption peaks at 275 and 314 nm, characteristic of protonated SHAM in its initial state[22]. When the pH was increased to ~9, the absorbance at 314 nm decreased while a new band at 334 nm emerged, indicative of the doubly deprotonated form of SHAM. This shift reflected the alkalinization-induced deprotonation, which disrupted the metal-ligand chelation and thereby reduced adhesion. Returning the solution to pH 5 restored the protonated form, re-establishing chelation and confirming a fully reversible adhesion cycle. The concomitant decrease in absorbance at 280 nm may be associated with dilution of DHMAAB. In contrast, catechol exhibited a single peak at 275 nm under neutral conditions (**Figure S13b**). Upon increasing the pH to ~9, its absorbance at 275 nm intensified while a broad band appeared between 400–600 nm, consistent with quinone formation[50, 51]. This oxidation accounted for the irreversible adhesion loss observed in CAT. Notably, the quinone band persisted after returning the solution to pH 5, confirming that catechol oxidation is largely irreversible and prevents adhesion recovery.

FTIR was employed to verify the molecular structures of SHA and CAT coatings before and after electrochemical deactivation and recovery treatments (**Figure 6**). Both copolymers exhibited characteristic signals of the MEA backbone (C=O at 1728 cm^{-1}) and aromatic ring associated with SHAM, catechol, or pyrene (C=C at 1448 cm^{-1} and 1512 cm^{-1}). In addition, the hydroxamic acid side chain in SHA was identified by the N-O stretching band at 1599 cm^{-1}, distinguishing SHA from CAT. For SHA, the FTIR spectra showed negligible changes in peak positions between the virgin, deactivated, and recovered states, indicating structural stability under the applied treatments. In contrast, CAT exhibited clear spectral changes following

View Article Online
DOI: 10.1039/D5SC07881D

deactivation. As shown in **Figure 6d**, the characteristic C-H bending peaks of catechol`s aromatic ring (806, 776, and 752 cm^{-1}) disappeared after charging at 1%V for 30 seconds and remained absent after attempted recovery. These results indicated irreversible oxidation of the aromatic ring to quinone, consistent with the observed loss of adhesion and failure to regain adhesive functionality.

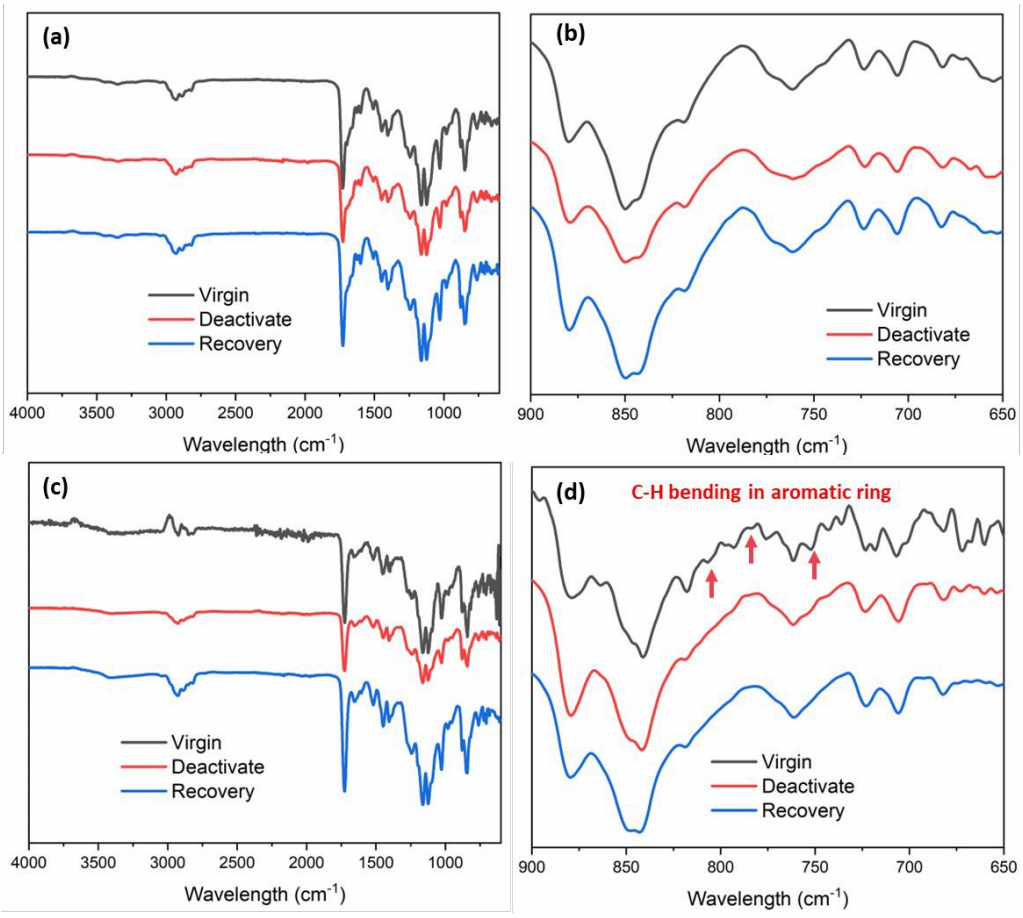

Figure 6. FTIR spectra of (a)(b) SHA and (c)(d) CAT coating after deactivating under 1 V potential for 30s and recover in pH 5 buffer for 30 mins. The red arrows in (d) are associated with the oxidation of catechol.

View Article Online
DOI: 10.1039/D5SC07881D

X-ray photoelectron spectroscopy (XPS) was conducted to analyze chemical changes in the adhesive coatings after electrochemical treatment and acidic recovery. The survey spectra indicated the presence of carbon, oxygen, and nitrogen (**Figure S14**). High-resolution C 1s spectra displayed minor variations (**Figure S15**, **Tables S3** and **S4**), but interpretation was complicated by the predominant C-C peak (~284.7 eV) resulting from overlapping contributions of the polymer backbone. The O 1s spectra showed distinct shifts related to SHAM and catechol oxygen functionalities (**Figure 7**, **Tables S5** and **S6**), offering direct insight into interfacial chemical changes. Four oxygen deconvoluted peaks were identified for SHA: hydroxamate carbonyl oxygen in -C(=**O**)-NHOH at 531.6-531.9 eV (1.5-2.5%, stable throughout), protonated hydroxamate (-C(=O)-N-**O**H) and phenolic hydroxyl groups (C_6H_4-**O**H) at 533-533.3 eV (68.23% in virgin)[52], high binding energy component assigned to deprotonated or weakly coordinated oxygen species including C(=O)-N-$\mathbf{O}^-$ and C_6H_4-$\mathbf{O}^-$ at 533.8-534.2 eV (4.02% in virgin)[52] and hydrogen-bonded interfacial oxygen associated with absorbed H_2O bonded to hydroxamate and phenol groups(534-535 eV; 25.22% in virgin)[53]. After electrochemical deactivation, the protonated hydroxamate/phenolic component reduced from 68.23% to 63.23%, which coincided with an increase in the deprotonated oxygen fraction from 4.02% to 14.10%. Upon reactivation in an acidic buffer, the protonated hydroxamate/phenolic oxygen recovered to 68.05% while the deprotonated oxygen reduced to the original 4.05%. These shifts in oxygen signals indicated the reversible nature of SHAM as a result of deprotonation and reprotonation of the SHAM hydroxinamic acid and phenol hydroxyl groups (C(=O)-N-OH → C(=O)-N–O^- → C(=O)-N–OH; C_6H_4-OH → C_6H_4-O^- → C_6H_4-OH) without irreversible oxidation. The

View Article Online
DOI: 10.1039/D5SC07881D

hydrogen-bonded oxygen component (534.3-534.7 eV) decreased from 25.22% to 20.15% after deactivation, likely due to a reduction in hydrogen bonding following the deprotonation of the -OH groups. It rose back to 26.34% when reactivated, near the virgin value and shows that hydrogen bonding at the surface has recovered[54].

Conversely, CAT was irreversibly oxidized as demonstrated by a decrease in the phenolic hydroxyl oxygen signal ($C_6H_4(\mathbf{O}H)_2$, 532.8-533.1 eV)[55] from 75.00% to 35.95% as a result of electrical stimulation and a lack of significant recovery when CAT was treated with an acidic buffered (38.11%). Coincidentally, quinone signal ($C_6H_4(=\mathbf{O})_2$, 531.3-531.7 eV)[56, 57] increased from 1.24% to 5.14% and only reduced slightly to 4.63%. The high energy oxygen peak at 534.0-534.5 eV is associated with phenolic hydroxyl or quinoid carbonyl groups bonded with water ($C_6H_4(\mathbf{O}H)_2\cdots$H-O-H and $C_6H_4(\mathbf{O}H)_2\cdots$H-O-H)[53, 54]. The high-binding-energy oxygen rose from 21.94 % to 41.70% and remained at 36.19% after acid treatment. This result suggests a rise in surface polarity and a stronger interaction between quinonoid carbonyl groups and surface moisture or adsorbed H_2O[58]. XPS spectra clearly indicated that catethol irreversibly oxidized to its poorly adhesive quinone form after electrical stimulation.

View Article Online
DOI: 10.1039/D5SC07881D

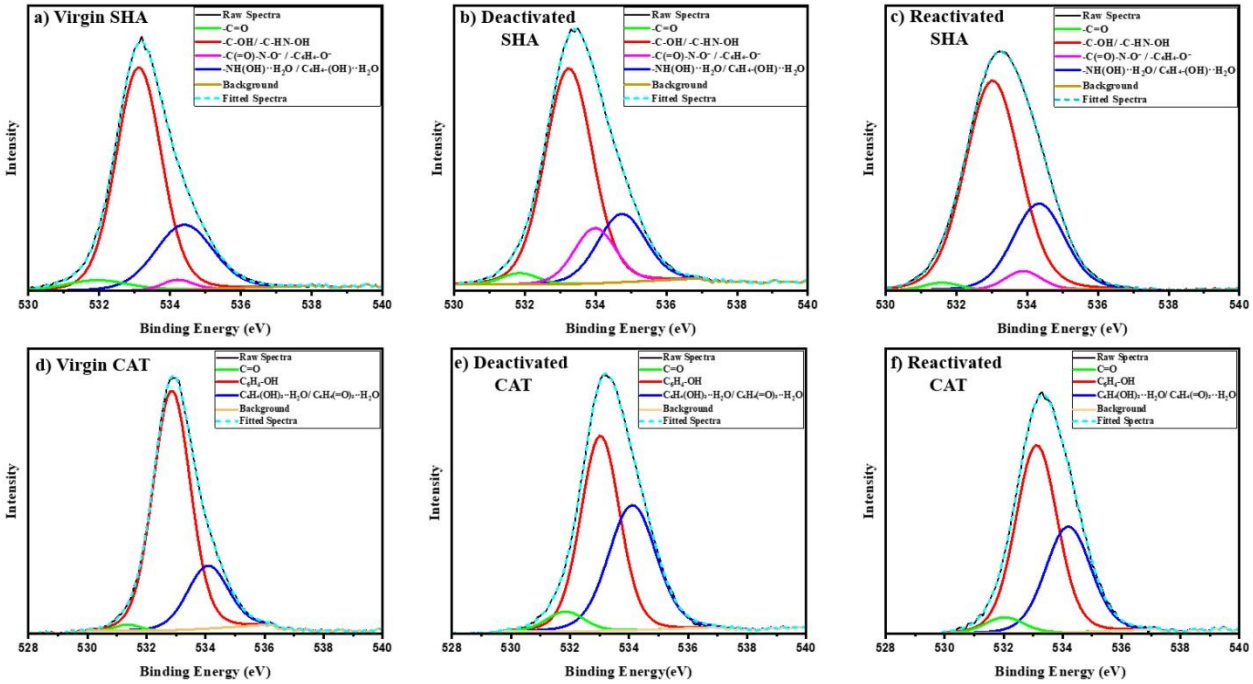

Figure 7. High-resolution O 1s XPS spectra of the SHA (a-c) and CAT (d-f) coatings in virgin (a,d), electrochemically deactivated (b,e), and reactivated states (c,f) featuring peak deconvolution.

Finally, the reversibility of the SHAM-based adhesive was evaluated through repeated deactivation-recovery cycles. The coating was subjected to 1%V for 30 seconds, followed by 30 minutes of incubation in pH 5 buffer. After each deactivation step, W_{adh} values decreased by 80-86% but consistently returned to the original value after recovery (**Figure 8**). No significant differences were observed compared with the initial adhesion performance. Up to five successful cycles were completed, confirming the reversible and repeatable electro-responsive behavior of the SHAM-based adhesive.

View Article Online
DOI: 10.1039/D5SC07881D

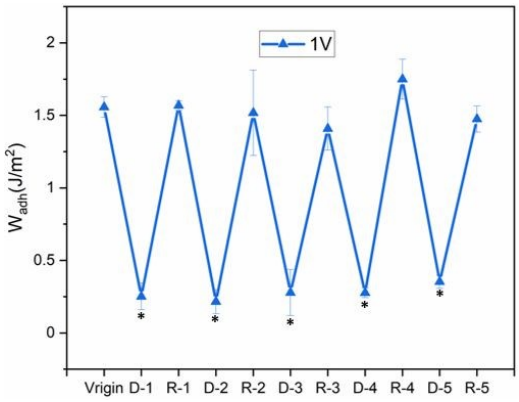

Figure 8. W_{adh} of SHA ested in successive contact cycles with the application of 1 V for 30 s (denoted as D) for the reduction of adhesive properties and incubation in pH 5 for 30 mins for recovering adhesion (denoted as R). Numerical values 1-5 represent the cycle number. *p < 0.05 when compared to the virgin adhesive properties.

In summary, SHAM demonstrated strong potential as an electrochemically controlled, switchable adhesive for metallic surfaces under wet conditions. CV and EIS results confirmed that SHA and CAT possess comparable electrical resistance, indicating that the observed differences in adhesion arose from the intrinsic electrochemical behavior of the adhesive monomers. In its protonated state, SHAM binds to the Ti surface primarily through the hydroxamate functional group, which is a strong chelator of metals [24, 25]. On Ti substrates, the hydroxamate group can coordinate through bidentate or bridging interactions involving the carbonyl oxygen and the N-O moiety, resulting in strong interfacial adhesion. Upon electrochemical charging, local alkalinization near the cathode leads to deprotonation of the hydroxamic acid. Deprotonation alters both the charge state and coordination geometry of the hydroxamate group, which weakens its affinity for Ti by disrupting optimal chelation and reducing the stability of the metal-ligand complex. This change in coordination is consistent with

View Article Online
DOI: 10.1039/D5SC07881D

the observed loss of adhesion during deactivation. Subsequent exposure to acidic conditions restores protonation of SHAM, re-establishing metal-ligand interactions and enabling recovery of adhesion.

SHAM underwent reversible deprotonation upon charging, followed by protonation in acidic media to restore strong adhesion. In contrast, catechol was irreversibly oxidized to quinone, preventing reduction and recovery under pH 5 conditions. Both adhesives can be deactivated using electrical potential as low as 0.5V, which is lower than the electrolytic voltage (1.23V) of water[59]. This low activation threshold is advantageous, as it prevents gas bubble formation, minimizes electrode corrosion, and reduces harmful byproducts such as hydrogen peroxide that accelerate metal degradation[60-64]. A key distinction between the two adhesive moieties lies in their reversibility. SHAM fully recovered its adhesive property after electrical stimulation, whereas catechol did not. It was previously demonstrated that catechol requires a temporary protecting group in the form of boronic acid to recover its initial adhesive property after electrochemical oxidation[20, 46]. This highlights SHAM's superior chemical stability when compared to catechol and its potential in functioning as a switchable adhesive molecule that responses to electrochemical control.

We compared the performance of SHAM with representative electricity responsive reversible adhesives reported in the literature (**Table S7**). When a protecting group in the form of phenylboronic acid is incorporated into catechol-containing adhesive, the adhesive system demonstrated responded to applied voltage in the range of 1-2V and with equivalent adhesive

View Article Online
DOI: 10.1039/D5SC07881D

performance[21]. However, this adhesive demonstrated higher switching ratio due to the formation of boronate complex to completely deactivate catechol adhesion. Electroadhesive consisting of polylectrolytes demonstrated high reversibility[65, 66]. However, the adhesive requires applied electricity to generate electrostatic interaction and is limited to bonding between ionic surfaces. Thermal responsive adhesives can be modified to respond to applied electricity through electrothermal heating effect, but these adhesive often suffers from long transition time[67]. SHAM reported here presents a new, alternative adhesive molecule for designing electroresponsive adhesive.

This study demonstrates that SHAM-based coatings can be directly deactivated on conductive substrates, with the substrate serving both as an electrode and as the adhesive contact surface. While this approach is effective, it restricts use for contacting nonconductive surfaces and a better integration of the counter electrode into the contacting surface may be required[20]. In the present study, reactivation required acidic incubation, which is not a practical trigger for real-world applications. We attempted to achieve recovery by reversing current direction. However, it was unsuccessful, likely due to ligand (SHAM) isomerization or continued electron transfer-induced chelate rearrangements, which disrupted SHAM-Ti binding[47, 48]. Future work will focus on confining the electrochemical reactions within the adhesive–circuit itself, enabling reversible adhesion control on a broader range of conductive and insulating substrates.

Despite these limitations, SHAM offers significant advantages over catechol, including stronger initial adhesion, robust reversibility without the need for protective groups, and stability

View Article Online
DOI: 10.1039/D5SC07881D

under basic conditions. These findings position SHAM as a promising adhesive molecule for designing electro-responsive, switchable adhesives for contacting wetted surfaces. Its tunable, low-voltage operation and repeatable reversibility open pathways for practical applications in reusable biomedical adhesives, minimally invasive wound dressings, wearable electronics, and underwater robotic manipulators, where precise and reversible adhesion is essential.

4. CONCLUSION

SHAM-containing adhesive exhibited electro-responsive and switchable interfacial bonding to metallic surfaces under wet conditions without the need for protecting groups. Adhesion could be effectively deactivated at voltages as low as 0.5 V within 30 seconds. Upon exposure to a mildly acidic pH environment, SHAM fully regained its initial adhesive strength owing to the reversible protonation-deprotonation reaction. In contrast, catechol-based adhesives suffered irreversible adhesion loss due to oxidative conversion to quinone, underscoring SHAM's superior chemical stability and reversibility. Its low-voltage activation, strong adhesion, and full reversibility make SHAM a promising candidate for reusable biomedical adhesives, wound dressings, wearable electronics, and underwater robotics requiring precise on-demand adhesion.

ASSOCIATED CONTENT

Supporting Information

The Supporting Information is available free of charge. NMR spectra, GPC characterization, FE-SEM characterization, and EIS spectra of two copolymers, UV-vis spectra of two monomers, representative contact curves of adhesive coatings influenced by electricity deactivation and pH driven reactivation.

View Article Online
DOI: 10.1039/D5SC07881D

Deactivation-recovery cycling of an electro-responsive SHAM adhesive (**Video S1**)

AUTHOR INFORMATION

Corresponding Authors

Bruce P. Lee − Biomedical Engineering Department, Michigan Technological University, 1400 Townsend Drive, Houghton, Michigan, 49931, United States; E-mail: bplee@mtu.edu

Authors

Kan Wang − Biomedical Engineering Department, Michigan Technological University, 1400 Townsend Drive, Houghton, Michigan, 49931, United States

Vedika Khare − Biomedical Engineering Department, Michigan Technological University, 1400 Townsend Drive, Houghton, Michigan, 49931, United States

Abhilash Arjan Das − Biomedical Engineering Department, Michigan Technological University, 1400 Townsend Drive, Houghton, Michigan, 49931, United States

Seyedehfatemeh Razaviamri − Biomedical Engineering Department, Michigan Technological University, 1400 Townsend Drive, Houghton, Michigan, 49931, United States

Author Contributions

K.W. contributed to conceptualization, visualization, and project administration. K.W., V.K., A.A.D., and F.R. contributed to methodology, investigation and formal analysis. B.P.L. contributed to conceptualization, supervision, and funding acquisition. All authors contributed to writing and editing the manuscript.

Funding Sources

View Article Online
DOI: 10.1039/D5SC07881D

This project was funded by the National Science Foundation under award number CMMI 2119019, the National Institutes of Health under award number R15GM135875, and the Office of Naval Research under award number N00014-21-1-2877. K.W. was funded in part by Health Research Institute (HRI) and Doctoral Finishing Fellowships from Michigan Technological University (MTU).

Notes

The authors declare no competing financial interest.

REFERENCES

1. Y. L. Tan, Y. J. Wong, N. W. X. Ong, Y. Leow, J. H. M. Wong, Y. J. Boo, R. Goh and X. J. Loh, Adhesion Evolution: Designing Smart Polymeric Adhesive Systems with On-Demand Reversible Switchability, *ACS Nano*, 2024, **18**, 24682-24704.
2. C. Xie, Y. Li, X. Guo, Y. Ding, X. Lu and S. Rao, Mussel-inspired adhesive hydrogels for local immunomodulation, *Materials Chemistry Frontiers*, 2023, **7**, 846-872.
3. C. Linghu, Y. Liu, X. Yang, Z. Chen, J. Feng, Y. Zhang, Y. Li, Z. Zhao, Y.-J. Seo and J. Li, Versatile adhesive skin enhances robotic interactions with the environment, *Science Advances*, 2025, **11**, eadt4765.
4. M. Wu, W. H. Afridi, J. Wu, R. H. Afridi, K. Wang, X. Zheng, C. Wang and G. Xie, Octopus-inspired underwater soft robotic gripper with crawling and swimming capabilities, *Research*, 2024, **7**, 0456.
5. H. Lee, D.-S. Um, Y. Lee, S. Lim, H.-j. Kim and H. Ko, Octopus-inspired smart adhesive pads for transfer printing of semiconducting nanomembranes, *Adv. Mater*, 2016, **28**, 7457-7465.
6. Z. Wang, L. Guo, H. Xiao, H. Cong and S. Wang, A reversible underwater glue based on photo- and thermo-responsive dynamic covalent bonds, *Materials Horizons*, 2020, **7**, 282-288.
7. D. K. Hohl and C. Weder, (De) bonding on demand with optically switchable adhesives, *Advanced Optical Materials*, 2019, **7**, 1900230.
8. C. Qin, H. Yang, B. Li, Z. Xing, B. Yu, M. Cai, X. Pei, Y. Ma, F. Zhou and W. Liu, Branched Oligomer-Based Reversible Adhesives Enabled by Controllable Self-Aggregation, *Adv. Mater.*, 2024, **36**, 2408330.
9. A. R. Narkar, B. Barker, M. Clisch, J. Jiang and B. P. Lee, pH Responsive and Oxidation Resistant Wet Adhesive based on Reversible Catechol–Boronate Complexation, *Chem. Mater.*, 2016, **28**, 5432-5439.
10. L. K. Borden, A. Gargava and S. R. Raghavan, Reversible electroadhesion of hydrogels to animal tissues for suture-less repair of cuts or tears, *Nature Communications*, 2021, **12**, 4419.

View Article Online
DOI: 10.1039/D5SC07881D

11. D. J. Levine, O. A. Lee, G. M. Campbell, M. K. McBride, H. J. Kim, K. T. Turner, R. C. Hayward and J. H. Pikul, A low-voltage, high-force capacity electroadhesive clutch based on ionoelastomer heterojunctions, *Adv. Mater.*, 2023, **35**, 2304455.
12. I.-D. Sîrbu, M. Bolignari, S. D'Avella, F. Damiani, L. Agostini, P. Tripicchio, R. Vertechy, L. Pancheri and M. Fontana, 2022.
13. C. Lee, H. Shi, J. Jung, B. Zheng, K. Wang, R. Tutika, R. Long, B. P. Lee, G. X. Gu and M. D. Bartlett, Bioinspired materials for underwater adhesion with pathways to switchability, *Cell Reports Physical Science*, 2023, **4**.
14. S. X. Wang and J. H. Waite, Catechol redox maintenance in mussel adhesion, *Nature Reviews Chemistry*, 2025, DOI: 10.1038/s41570-024-00673-4.
15. Y. Ma, B. Zhang, I. Frenkel, Z. Zhang, X. Pei, F. Zhou and X. He, in *Progress in Adhesion and Adhesives*, 2021, DOI: https://doi.org/10.1002/9781119846703.ch17, pp. 739-759.
16. Q. Guo, J. Chen, J. Wang, H. Zeng and J. Yu, Recent progress in synthesis and application of mussel-inspired adhesives, *Nanoscale*, 2020, **12**, 1307-1324.
17. H. Lee, N. F. Scherer and P. B. Messersmith, Single Molecule Mechanics of Mussel Adhesion, *Proc. Natl. Acad. Sci. USA*, 2006, **103**, 12999-13003.
18. M. S. Akram Bhuiyan, J. D. Roland, B. Liu, M. Reaume, Z. Zhang, J. D. Kelley and B. P. Lee, In Situ Deactivation of Catechol-Containing Adhesive Using Electrochemistry, *J. Am. Chem. Soc.* , 2020, **142**, 4631-4638.
19. S. Shahrokhian and A. Hamzehloei, Electrochemical oxidation of catechol in the presence of 2-thiouracil: application to electro-organic synthesis, *Electrochem. Commun.*, 2003, **5**, 706-710.
20. M. S. A. Bhuiyan, J. Manuel, F. Razaviamri and B. P. Lee, Electrochemical deactivation of switchable catechol-containing smart adhesive from nonconductive surfaces, *ACS Applied Polymer Materials*, 2023, **5**, 3949-3957.
21. M. S. A. Bhuiyan, B. Liu, J. Manuel, B. Zhao and B. P. Lee, Effect of conductivity on in situ deactivation of catechol–boronate complexation-based reversible smart adhesive, *Biomacromolecules*, 2021, **22**, 4004-4015.
22. K. Wang, L. Patra, B. Liu, Z. Zhang, R. Pandey and B. P. Lee, Salicylhydroxamic acid as a novel switchable adhesive molecule, *Chem. Mater.*, 2023, **35**, 5322-5330.
23. M. S. A. Bhuiyan, K. Wang, F. Razaviamri and B. P. Lee, Salicylhydroxamic acid containing structural adhesive, *RSC applied polymers*, 2024, **2**, 838-846.
24. J. P. Meszaros, H. Kovács, G. Spengler, F. Kovács, E. Frank and E. A. Enyedy, A comparative study on the metal complexes of an anticancer estradiol-hydroxamate conjugate and salicylhydroxamic acid, *J. Inorg. Biochem.*, 2023, **244**, 112223.
25. H. Liu, W. Zhao, J. Zhai, X. Lu, P. Chen, X. Ren, W. Sun, C. Zhang, W. Chen and S. Wan, Activation mechanism of lead (II) to ilmenite flotation using salicylhydroxamic acid as collector, *Minerals*, 2020, **10**, 567.
26. S. Marini, P. Salvi, P. Nelli, R. Pesenti, M. Villa, M. Berrettoni, G. Zangari and Y. Kiros, Advanced alkaline water electrolysis, *Electrochimica Acta*, 2012, **82**, 384-391.
27. M. Wang, Z. Wang, X. Gong and Z. Guo, The intensification technologies to water electrolysis for hydrogen production–A review, *Renewable and sustainable energy reviews*, 2014, **29**, 573-588.
28. M. Ciavarella, J. Joe, A. Papangelo and J. Barber, The role of adhesion in contact mechanics, *Journal of the Royal Society Interface*, 2019, **16**, 20180738.

View Article Online
DOI: 10.1039/D5SC07881D

29. K. R. Shull, Contact mechanics and the adhesion of soft solids, *Materials Science and Engineering: R: Reports*, 2002, **36**, 1-45.
30. S. T. Choi, Extended JKR theory on adhesive contact of a spherical tip onto a film on a substrate, *Journal of Materials Research*, 2012, **27**, 113-120.
31. B. P. Lee, K. Huang, F. N. Nunalee, K. R. Shull and P. B. Messersmith, Synthesis of 3,4-Dihydroxyphenylalanine (DOPA) Containing Monomers and Their Copolymerization with PEG-Diacrylate to from Hydrogels, *J. Biomater. Sci., Polym. Ed.*, 2004, **15**, 449-464.
32. K. R. Shull, Contact mechanics and the adhesion of soft solids, *Matrl. Sci. Eng. R. Rep.*, 2002, **R36**, 1-45.
33. N. Elgrishi, K. J. Rountree, B. D. McCarthy, E. S. Rountree, T. T. Eisenhart and J. L. Dempsey, A practical beginner's guide to cyclic voltammetry, *Journal of chemical education*, 2018, **95**, 197-206.
34. A. C. Lazanas and M. I. Prodromidis, Electrochemical impedance spectroscopy─ a tutorial, *ACS measurement science au*, 2023, **3**, 162-193.
35. G. M. da Silva, P. M. Faia, S. R. Mendes and E. S. Araujo, A review of impedance spectroscopy technique: applications, modelling, and case study of relative humidity sensors development, *Applied Sciences*, 2024, **14**, 5754.
36. L. Zhao, Z. Sun, H. Zhang, Y. Li, Y. Mo, F. Yu and Y. Chen, An environment-friendly crosslinked binder endowing LiFePO 4 electrode with structural integrity and long cycle life performance, *RSC advances*, 2020, **10**, 29362-29372.
37. J. L. Carter, C. A. Kelly, J. E. Marshall and M. J. Jenkins, Effect of thickness on the electrical properties of PEDOT: PSS/Tween 80 films, *Polym. J.*, 2024, **56**, 107-114.
38. F. Czerwinski, Aluminum alloys for electrical engineering: a review, *JMatS*, 2024, **59**, 14847-14892.
39. X. Atanacio-Sánchez, C. G. Garay-Reyes, A. Martínez-García, I. Estrada-Guel, J. M. Mendoza-Duarte, P. Guerrero-Seañez, S. González-Sánchez, E. Rocha-Rangel, J. de Jesús Cruz-Rivera and E. J. Gutiérrez-Castañeda, Enhancement of the Electrical Conductivity and Mechanical Properties of Al-Mg-Si and Al-Mg-Zn Ternary Systems After a T8 Heat Treatment, *Metals*, 2024, **14**, 1286.
40. Y. Wang, Y. Xue, M. Pan and S. Wen, Interaction of salicylhydroxamic acid with the surface of MgTi2O5: a study combined DFT and experiment, *Journal of Alloys and Compounds*, 2019, **774**, 222-228.
41. B. Wang and X. Luo, A first-principles study on potential chelation agents and indicators of Alzheimer's disease, *RSC Advances*, 2020, **10**, 35574-35581.
42. J. Yang, P. J. Bremer, I. L. Lamont and A. J. McQuillan, Infrared spectroscopic studies of siderophore-related hydroxamic acid ligands adsorbed on titanium dioxide, *Langmuir*, 2006, **22**, 10109-10117.
43. E. C. O'Brien, Metal complexes of salicylhydroxamic acid (H2Sha), anthranilic hydroxamic acid and benzohydroxamic acid. Crystal and molecular structure of [Cu(phen)2(Cl)]Cl·H2Sha, a model for a peroxidase-inhibitor complex, *Journal of Inorganic Biochemistry*, 2000, DOI: https://doi.org/10.1016/S0162-0134(99)00245-7.
44. B. M. O. Salama, A COMPARATIVE STUDY OF OPTIMIZATION METHODS FOR EDDY-CURRENT CHARACTERIZATION OF AERONAUTICAL METAL SHEETS, *Electronics and Energetics*, 2021, DOI: https://doi.org/10.2298/FUEE2104547S.

View Article Online
DOI: 10.1039/D5SC07881D

45. I. Bibi, A comprehensive study of electrically switchable adhesives: Bonding and debonding on demand, *Materials Today Communications*, 2023, DOI: https://doi.org/10.1016/j.mtcomm.2023.106293.
46. J. Huang, Y. Liu, Y. Yang, Z. Zhou, J. Mao, T. Wu, J. Liu, Q. Cai, C. Peng, Y. Xu, B. Zeng, W. Luo, G. Chen, C. Yuan and L. Dai, Electrically Programmable Adhesive Hydrogels for Climbing Robots An electrochemical route to adhesion control, *Science Robotics*, 2021.
47. A. R. Kottaichamy, M. A. Nazrulla, M. Parmar, R. Thimmappa, M. C. Devendrachari, C. P. Vinod, M. Volokh, H. M. N. Kotresh, M. Shalom and M. O. Thotiyl, Ligand isomerization driven electrocatalytic switching, *Angew. Chem. Int. Ed.*, 2024, **63**, e202405664.
48. V. Ovcharenko, O. Kuznetsova, E. Fursova, G. Romanenko, A. Polushkin and R. Sagdeev, Redox-induced change in the ligand coordination mode, *Inorganic Chemistry*, 2014, **53**, 10033-10035.
49. S. Mazloomi and N. Sulaiman, Influencing factors of water electrolysis electrical efficiency, *Renewable and Sustainable Energy Reviews*, 2012, **16**, 4257-4263.
50. S. Goia, G. W. Richings, M. A. Turner, J. M. Woolley, J. J. Tully, S. J. Cobb, A. Burriss, B. R. Robinson, J. V. Macpherson and V. G. Stavros, Ultrafast spectroelectrochemistry of the catechol/o-quinone redox couple in aqueous buffer solution, *ChemPhotoChem*, 2024, **8**, e202300325.
51. N. Vân Anh and R. M. Williams, Bis-semiquinone (bi-radical) formation by photoinduced proton coupled electron transfer in covalently linked catechol-quinone systems: Aviram's hemiquinones revisited, *Photochemical & Photobiological Sciences*, 2012, **11**, 957-961.
52. Q. Wang, Y. Wang, Y. Wu, J. Li, J. Peng, S. Ma and M. Zhai, Salicylhydroxamic acid intercalated layered double hydroxide for efficient uranium uptake from seawater, *Journal of Environmental Chemical Engineering*, 2025, **13**, 115055.
53. D. V. Sivkov, O. V. Petrova, S. V. Nekipelov, A. S. Vinogradov, R. N. Skandakov, K. A. Bakina, S. I. Isaenko, A. M. Ob'edkov, B. S. Kaverin and I. V. Vilkov, Quantitative characterization of oxygen-containing groups on the surface of carbon materials: XPS and NEXAFS study, *Applied Sciences*, 2022, **12**, 7744.
54. S. Kerber, J. Bruckner, K. Wozniak, S. Seal, S. Hardcastle and T. Barr, The nature of hydrogen in x-ray photoelectron spectroscopy: general patterns from hydroxides to hydrogen bonding, *Journal of Vacuum Science & Technology A: Vacuum, Surfaces, and Films*, 1996, **14**, 1314-1320.
55. J. Wang, W. Guo, K. Tian, X. Li, X. Wang, P. Li, Y. Zhang, B. Zhang, B. Zhang and S. Liu, Proof of aerobically autoxidized self-charge concept based on single catechol-enriched carbon cathode material, *Nano-Micro Letters*, 2024, **16**, 62.
56. B. Maiti, E. V. Van der Eycken and G. A. Coppola, Catechol modification as a platform for functional coatings, *Biomaterials Science*, 2025.
57. A. C. Gómez-Herrero, C. Sánchez-Sánchez, F. Chérioux, J. I. Martínez, J. Abad, L. Floreano, A. Verdini, A. Cossaro, E. Mazaleyrat and V. Guisset, Copper-assisted oxidation of catechols into quinone derivatives, *Chemical Science*, 2021, **12**, 2257-2267.
58. S. A. Mian, L.-M. Yang, L. C. Saha, E. Ahmed, M. Ajmal and E. Ganz, A fundamental understanding of catechol and water adsorption on a hydrophilic silica surface: exploring the underwater adhesion mechanism of mussels on an atomic scale, *Langmuir*, 2014, **30**, 6906-6914.
59. A. J. Shih, M. C. Monteiro, F. Dattila, D. Pavesi, M. Philips, A. H. da Silva, R. E. Vos, K. Ojha, S. Park and O. van der Heijden, Water electrolysis, *Nature Reviews Methods Primers*, 2022, **2**, 84.

View Article Online
DOI: 10.1039/D5SC07881D

60. H. Jang, S. Chung and J. Lee, In situ demonstration of anodic interface degradation during water electrolysis: corrosion and passivation, *Electrochimica Acta*, 2021, **365**, 137276.
61. M. M. Rashid, M. K. Al Mesfer, H. Naseem and M. Danish, Hydrogen production by water electrolysis: a review of alkaline water electrolysis, PEM water electrolysis and high temperature water electrolysis, *Int. J. Eng. Adv. Technol*, 2015, **4**, 2249-8958.
62. T. Naito, T. Shinagawa, T. Nishimoto and K. Takanabe, Water electrolysis in saturated phosphate buffer at neutral pH, *ChemSusChem*, 2020, **13**, 5921-5933.
63. G. Wang, J. Chen, Y. Li, J. Jia, P. Cai and Z. Wen, Energy-efficient electrolytic hydrogen production assisted by coupling urea oxidation with a pH-gradient concentration cell, *Chemical Communications*, 2018, **54**, 2603-2606.
64. C. Belmont, R. Ferrigno, O. Leclerc and H. Girault, Coplanar interdigitated band electrodes for electrosynthesis. Part 4: Application to sea water electrolysis, *Electrochimica Acta*, 1998, **44**, 597-603.
65. H. J. Kim, L. Paquin, C. W. Barney, S. So, B. Chen, Z. Suo, A. J. Crosby and R. C. Hayward, Low-Voltage Reversible Electroadhesion of Ionoelastomer Junctions, *Adv. Mat.*, 2020, **32**, 2000600.
66. S. Lu, Z. Ma, M. Ding, Y. Wu, Y. Chen, M. Dong and L. Qin, Reversible electroadhesion induced through low ion concentration migration for biomedical applications, *Chemical Engineering Journal*, 2024, **486**, 150393.
67. Q. Deng, S. Han, Y. Wu, Y. Chen, Y. Zhang, Y. Zhao, S. Chen and J. Zhu, Robust and Reversible Thermal/Electro-Responsive Supramolecular Polymeric Adhesives via Synergistic Hydrogen-Bonds and Ionic Junctions, *Angew. Chem., Int. Ed.*, 2025, **64**, e202415386.

View Article Online
DOI: 10.1039/D5SC07881D

The data supporting this article have been included as part of the Supplementary Information. Supplementary information: Tables S1-S6, NMR spectra (Figures S4 and S5), EIS Nyquist plot (Figure S6), JKR contact curves (Figures S8-S10), UV-vis spectra (Figure S13), and XPS spectra (Figures S14 and S15). See DOI: [URL – format https://doi.org/DOI]